Supporting Information

Huang et al. 10.1073/pnas.1311477111

SI Materials and Methods

Materials and Chemicals. Materials and chemicals include hydrogen tetrachloroaurate (III) hydrate ($HAuCl_4 \cdot 3H_2O$, 99.999%), sodium borohydride ($NaBH_4$, 99.99%), silver nitrate ($AgNO_3$, >99.0%), and poly(acrylic acid) sodium salt, M_r of ~15,000 (35 wt% solution in H_2O) (PAA). Cetyltrimethylammonium bromide (CTAB) (>99%) and ascorbic acid ($C_6H_8O_6$, >99.0%) were purchased from Sigma Chemical. Sodium chloride (>99.0%) was obtained from Fischer Chemicals. All of these reagents were used without any further purification. All solutions were prepared using Barnstead E-Pure 18-MΩ water.

Gold Nanorods Synthesis and Coating. Gold nanorods with different aspect ratios were synthesized using a seed-mediated silver-assisted method (1). First, Au seeds with diameter ~2–4 nm were synthesized by adding 0.6 mL of 0.01 M ice-cold $NaBH_4$ solution into a mixture of 0.25 mL of 0.01 M $HAuCl_4$ aqueous solution and 9.75 mL of 0.1 M CTAB aqueous solution, followed by vigorous stirring for 10 min. The prepared brownish Au seed solution stood for 30 min before use. Au nanorod (AuNR) growth solutions were prepared by mixing 0.5 mL of 0.01 M $HAuCl_4$ solution, 9.5 mL of 0.1 M CTAB solution, and 0.01 or 0.05 or 0.1 mL of 0.01 M $AgNO_3$ solution. Then 0.055 mL of 0.1 M ascorbic acid solution as reducing agent was added into the growth solution, and 0.012 mL of Au seed solution was added and the solution was allowed to stand overnight. The as-made AuNR solution was purified twice by centrifugation at $13{,}528 \times g$ for 20 min to remove excess surfactants and other reactants. AuNRs coated with PAA were prepared by electrostatic adsorption (2). Solutions of 1 mL of 0.01 M NaCl solution and 2 mL of 10 $mg \cdot mL^{-1}$ PAA were added into 10 mL of 0.5 nM AuNR solutions and shaken for 2 h. The solution was then purified by centrifugation at $7{,}155 \times g$ for 20 min and redispersed in deionized water to make the AuNR concentration at 5 nM with ~67% absorption at 785 nm for the aspect ratio-3.8 AuNRs.

Data for the 1.3-ps Pulse Excitations

Fig. S1 shows data and analysis for the 1.3-ps pulse duration that corresponds to the data for 0.45-ps pulse duration shown in Figs. 2*B* and 4*A*.

The Laser Pulse Shape and Duration

We measured the temporal shape of the laser pulse using a conventional autocorrelator. The autocorrelation has a FWHM of 0.65 ps and is described well by a Gaussian pulse shape (Eq. **S1**). $P(t)$ is the time-dependent laser power intensity in one laser pulse that appears in Eqs. **5** and **6**. We were unable to measure the autocorrelation of the pulse after the etalon and therefore used two-photon absorption (TPA) in a GaP detector to measure the correlation of the pulse after the etalon with a much shorter pulse that does not pass through the etalon. We determine the pulse shape after the etalon by convoluting the correlation. The resulting pulse shape is fit by a phenomenological equation that combines a broadened onset with an exponential decay (Eq. **S2**):

$$P(t) = \frac{Q}{\xi\sqrt{2\pi}} \exp\left(-\frac{t^2}{2\xi^2}\right), \qquad \textbf{[S1]}$$

$$P(t) = \frac{Q}{\eta} \frac{\exp(-t/\tau_1)}{\exp(-t/\tau_2)+1}. \qquad \textbf{[S2]}$$

In Eq. **S1**, the pulse has a Gaussian shape, Q is the energy in one laser pulse, r_0 is the $1/e^2$ intensity radius of the focused laser spot radius, and $\xi = 0.19$ ps is the temporal SD of the pulse. This choice of ξ is equivalent to a FWHM of 0.45 ps and an autocorrelation time 0.65 ps. We also calculated the fitting with a sech^2 shape pulse with the same autocorrelation time 0.65 ps, which generates a FWHM of 0.42 ps; the calculation of ΔT_{eff} shows nearly no difference from the calculation using a Gaussian shape pulse. Pulses that travel through the etalon are described by Eq. **S2** with $\tau_1 = 1.2$ ps, $\tau_2 = 0.1$ ps, and $\eta = 1.245$ ps. The FWHM of these pulses is 1.3 ps.

The temporal pulse shapes of these two cases are plotted as Fig. S2*A* and the evolution of electron temperature for the two cases are plotted as Fig. S2*B*.

Ratio of Pulsed vs. Continuous-Wave Emission Spectra

Fig. S3 summarizes the measured ratio of pulsed vs. continuous-wave (cw) emission spectra with comparisons to the ratio calculated using Eqs. **3** and **4** using a fixed value of the optical absorption cross-section. The experimental and calculated ratios generally match well on the anti-Stokes side. At large anti-Stokes shifts, the ratio is noisy because of the weak cw emission at $\Delta\omega < -1{,}500$ cm^{-1}. The ratios on the Stokes side match at low average laser power but deviate strongly at 2- and 4-mW excitation.

The T_{eff} Calculation on the Stokes Side. On the Stokes side, $\Delta\omega$ are of positive values. The Stokes intensity at $\Delta\omega$ is proportional to the following:

$$\begin{aligned} n(-\Delta\omega)+1 &= \left(\exp\left(hc\Delta\omega/k_B T_{eff}\right)-1\right)^{-1}+1 \\ &= \frac{\exp\left(hc\Delta\omega/k_B T_{eff}\right)}{\exp\left(hc\Delta\omega/k_B T_{eff}\right)-1} \\ &= \frac{1}{1-\exp\left(-hc\Delta\omega/k_B T_{eff}\right)}. \end{aligned} \qquad \textbf{[S3]}$$

Thus, the T_{eff} on the Stokes side can also be calculated with Eq. **4**.

Spectral Range of Scattering. In conventional electronic Raman scattering by bulk metals, momentum conservation is usually thought to introduce a cutoff at a frequency shift of v_F/δ, where v_F is the Fermi velocity and δ is the optical absorption length (3). For Au at 785 nm ($v_F = 1.4 \times 10^6$ $m \cdot s^{-1}$, $\delta = 13$ nm), this cutoff would be at ~570 cm^{-1}. (For a nanoparticle, we can expect that δ would be replaced by the geometry of the particle, e.g., the diameter; in our case, the diameter and the optical absorption length are similar.) We do not, however, observe an obvious cutoff in the scattering spectra. This is in agreement with the recent study of electronic Raman scattering by bulk metals where the spectra extend, in most cases, to >3,000 cm^{-1} (3).

The AuNR Emission Spectra by Two-Pulse Excitation

The emission spectra below in Fig. S4 are excited by two 0.45-ps laser pulses at different delay times. The spectrum intensity increase when the two laser pulses become more overlapped in time. Data presented in Fig. 5 are calculated based on the integrated

intensity ratio at a certain delay time vs. −10-ps delay time either in −400 to −600 cm^{-1} range or −800 to −1,000 cm^{-1} range.

Emission Spectra at Short Wavelengths

For completeness, we report the emission spectra at shorter wavelengths (500–750 nm) in Fig. S5 *A* and *B*. The signal generated by cw excitation is too weak at shorter wavelengths for us to apply the quantitative analysis scheme we used at longer wavelengths described by Eqs. **3** and **4** and summarized in Fig. 4 *B* and *C*. The best we can do at shorter wavelengths is compare the scaling of the emission intensity predicted by the electronic Raman scattering model as a function of laser power and laser pulse duration, see Fig. S5*C*. A model for the emission based on TPA followed by fluorescence would have a quadratic dependence on power, shown as a dashed line in Fig. S5*C*, and would predict a decrease by a factor of 3.5 in going from the 0.45-ps pulse duration to the 1.3-ps pulse duration at constant laser power. (The factor of 3.5 comes from the ratio of the integral of the intensity squared for these two pulse shapes.) We cannot conclusively distinguish between the two models (electronic Raman scattering vs. TPA followed by fluorescence) in the short wavelength range based on this scaling analysis alone.

1. Sau TK, Murphy CJ (2004) Seeded high yield synthesis of short Au nanorods in aqueous solution. *Langmuir* 20(15):6414–6420.
2. Gole A, Murphy CJ (2005) Polyelectrolyte-coated gold nanorods: Synthesis, characterization and immobilization. *Chem Mater* 17(6):1325–1330.
3. Ponosov YS, Streltsov SV (2012) Measurements of Raman scattering by electrons in metals: The effects of electron-phonon coupling. *Phys Rev B* 86(4):045138.

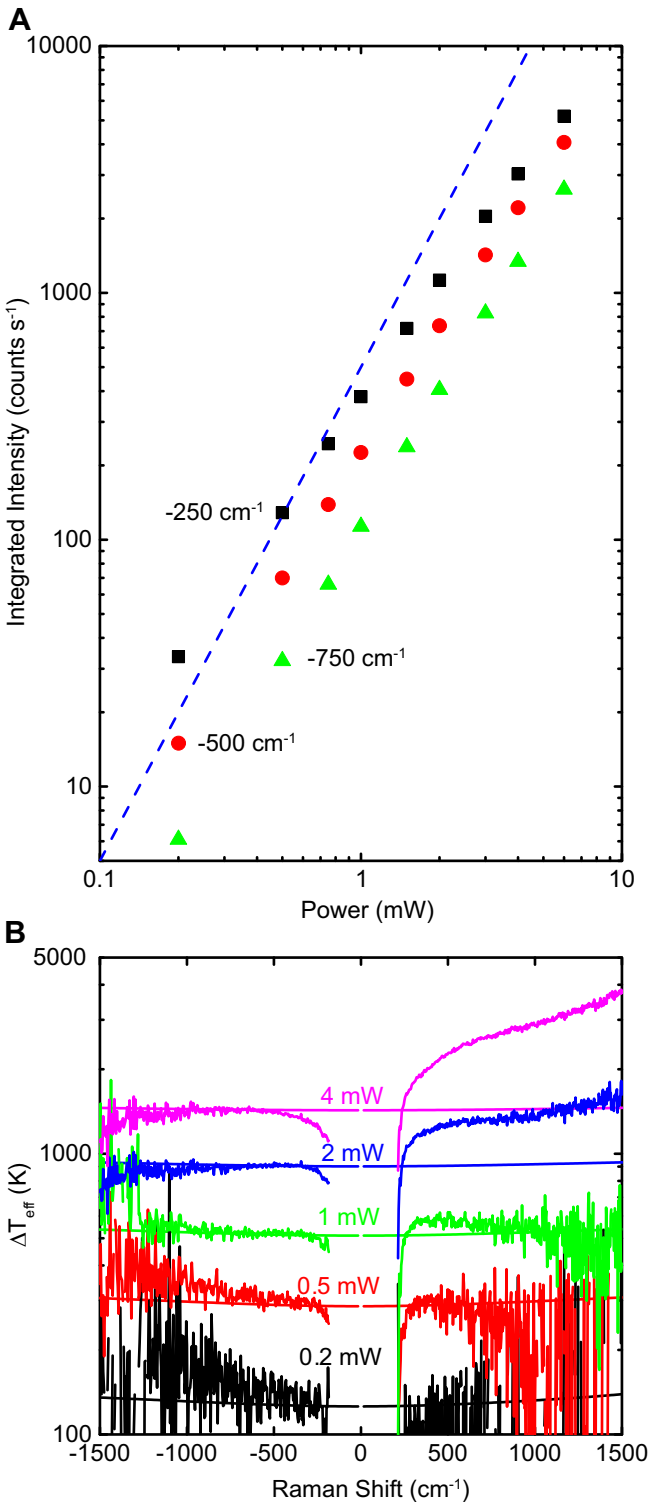

Fig. S1. (*A*) Raman scattering intensity vs. average incident power for AuNRs with absorption peak at 787 nm excited by pulsed 785-nm laser pulses of 1.3-ps width integrated over a Raman shift range of −240 to −260 cm^{-1} (black squares), −490 to −510 cm^{-1} (red circles), and −740 to −760 cm^{-1} (green triangles). The blue dashed line with a slope of 2 indicates a quadratic relation between the spectral intensity and average incident power. (*B*) Change in the effective temperature relative to room temperature $\Delta T_{eff} = T_{eff} - 300$ K of anti-Stokes Raman scattering by AuNRs with absorption peak at 787 nm excited by laser pulses of 1.3-ps width. ΔT_{eff} calculated from the data using Eq. **4** are shown as lines that show some noise. ΔT_{eff} calculated using Eqs. **4** and **6** with the optical cross-section $\sigma_{abss} = 2{,}700$ nm^2 (as determined in the 0.45-ps dataset) are shown as smooth lines.

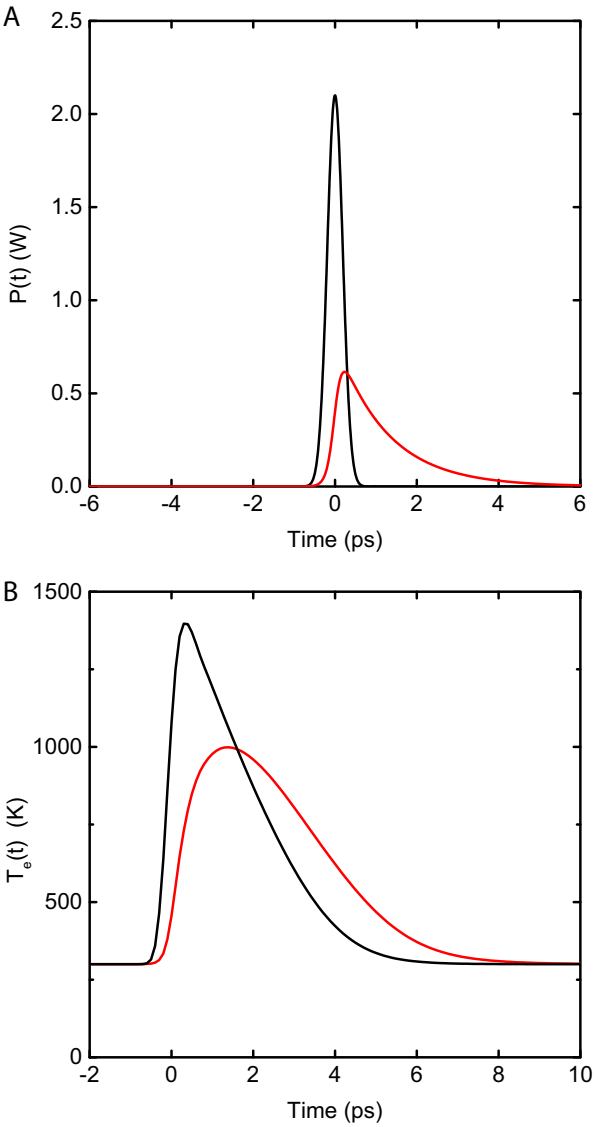

Fig. S2. (*A*) Laser pulse shapes calculated by Eqs. **S1** and **S2** for Gaussian pulse with FWHM = 0.45 ps (black) and the pulse with FWHM = 1.3 ps (red) after traveling through the etalon. The average laser power is 1 mW in both cases. (*B*) Evolution of the AuNR electron temperature during one laser pulse excitation calculated by Eq. **5** and Eqs. **S1** and **S2**. Pulse with 0.45-ps width (black); pulse with 1.3-ps width (red).

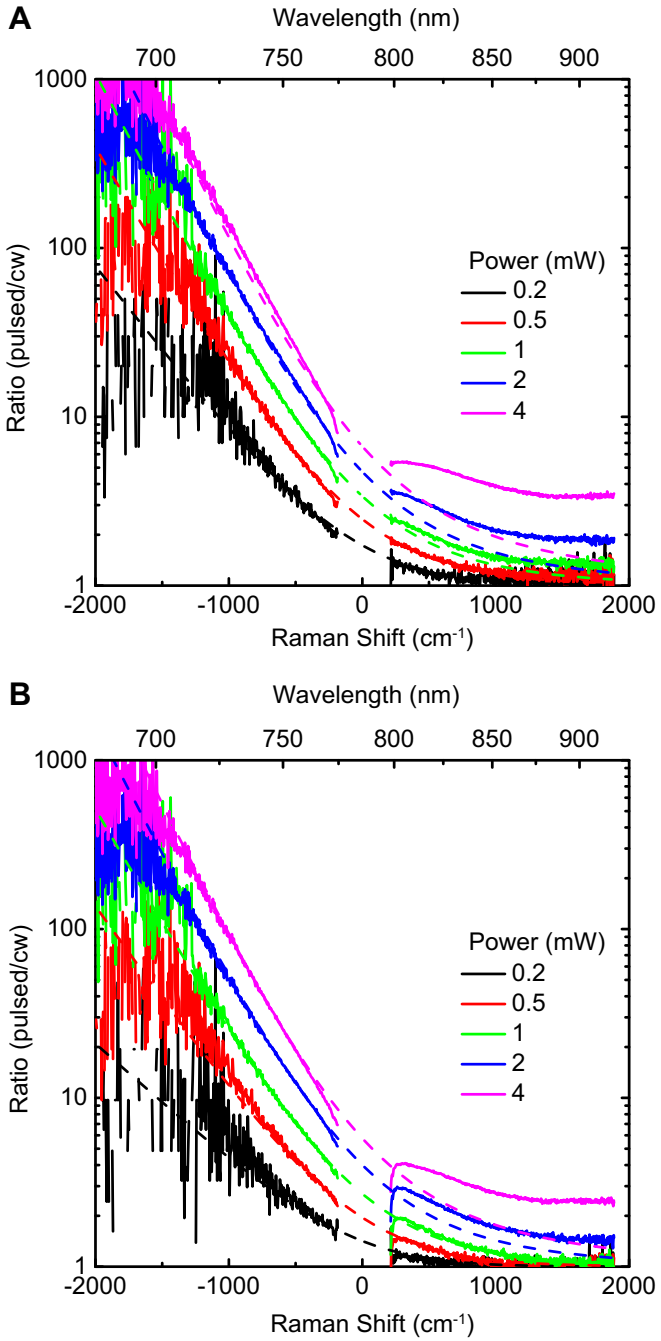

Fig. S3. Ratio of the normalized emission spectra (*S*/*P*) of aspect ratio-3.8 AuNRs excited by 785-nm laser of different average laser powers at pulsed mode with (*A*) 0.45-ps pulse width or (*B*) 1.3-ps pulse width vs. at cw mode (solid curves: data; dashed lines: calculated from Eqs. **5** and **6** with σ_{abs} = 2,700 nm^2).

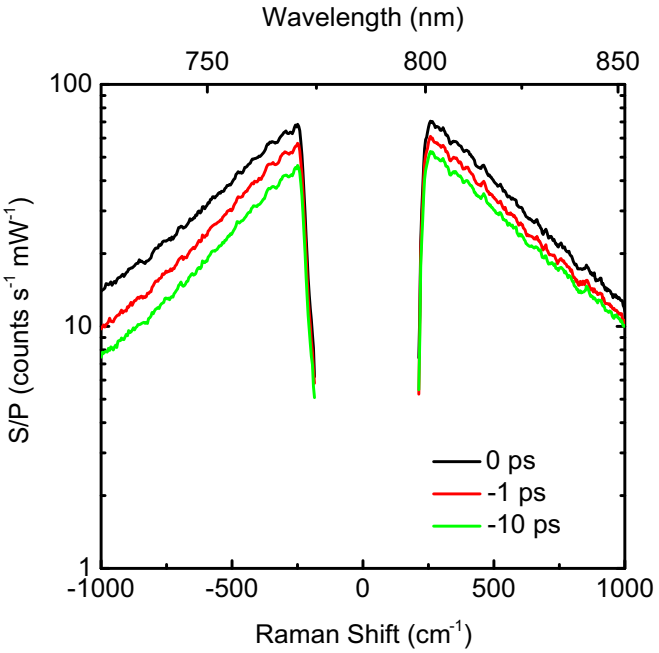

Fig. S4. Emission spectra of aspect ratio-3.8 AuNRs excited by two 0.45-ps laser pulses at different delay times. These spectra are not corrected for variations in the efficiency of the spectrometer. The short period oscillations in the data as a function of frequency shift are caused by variations in the quantum efficiency of the CCD sensor.

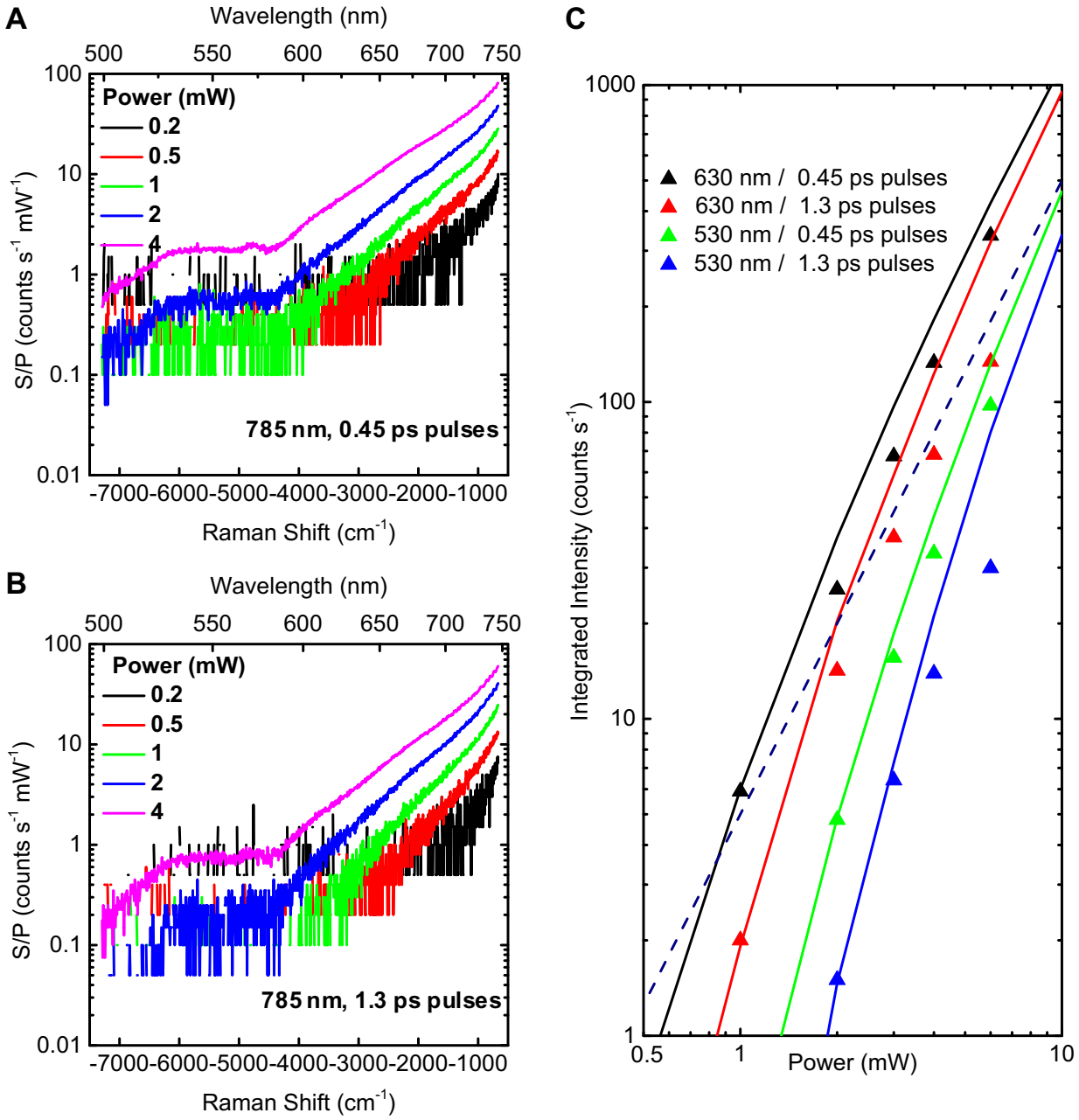

Fig. S5. Emission spectra of aspect ratio-3.8 AuNRs excited by 785-nm laser of different powers at pulsed mode (*A*) with pulse duration of 0.45 ps; (*B*) with pulse duration of 1.3 ps. (*C*) Integrated spectral intensity over a 20-nm-wide interval centered at 630 and 530 nm excited by either 0.45- and 1.3-ps duration pulses. The solid lines with colors keyed to the symbols indicate the relative spectral intensity calculated from Eqs. **1–3**. The values of T_{eff} at 630 and 530 nm using either 0.45- or 1.3-ps duration pulses are calculated with Eqs. **6** and **4**. Because the value of β in Eq. **1** is not the same at the two wavelengths of emission, we scale the calculated spectral intensity at 630 nm to fit the experimental value at 1 mW and 0.45-ps excitation, and scale the intensity at 530 nm to fit the experimental value at 2 mW and 0.45-ps excitation. Experimental signals at low laser powers with the values smaller than five times of the background values are excluded from the figure. The dashed line denotes a quadratic relation of intensity vs. power.